Int J Fract (2011) 167:33–45
DOI 10.1007/s10704-010-9515-4

ORIGINAL PAPER

The influence of the cohesive process zone in hydraulic fracturing modelling

E. Sarris · P. Papanastasiou

Received: 11 February 2010 / Accepted: 2 June 2010 / Published online: 25 June 2010

Abstract This paper studies the importance of the cohesive zone in the modelling of a fluid driven fracture under plain strain conditions. The fracture is driven by pumping of an incompressible viscous fluid at the fracture inlet. Rock deformation is modeled for linear elastic and poroelastic solids. Fluid flow in the fracture is modeled by lubrication theory. The cohesive zone approach is used as the fracture propagation criterion. Finite element analysis was used to compute the solution for the crack length, the fracture opening and propagation pressure as a function of the time and distance from the wellbore. It is demonstrated that the crack profiles and the propagation pressures are larger in the case of elastic-softening cohesive model compared to the results of the rigid-softening cohesive model for both elastic and poroelastic cohesive solids. It is found that the results are affected by the slope of the loading branch of the cohesive model and they are nearly unaffected from the exact form of the softening branch. Furthermore, the size of the process zone, the fracture geometry and the propagation pressure increase with increasing confining stresses. These results may explain partially the discrepancies in net-pressures between field measurements and conventional model predictions.

Keywords Hydraulic fracturing · Cohesive zone · Net-Pressures · Poroelasticity · Finite Elements

E. Sarris · P. Papanastasiou (✉)
Department of Civil and Environmental Engineering, University of Cyprus, P.O. BOX 20537, 1678 Nicosia, Cyprus
e-mail: panospap@ucy.ac.cy

E. Sarris
e-mail: esarris@ucy.ac.cy

1 Introduction

The mathematical problem of a fluid driven fracture arises in hydraulic fracturing, a technique widely used in the petroleum industry to enhance the recovery of hydrocarbons from underground reservoirs. Some other related applications in geomechanics include the magma-driven fractures (Spence and Turcotte 1985), the preconditioning of rock masses in mining operations to promote caving (Jeffrey et al. 2001), the formation of barriers to stop contaminant transport in environmental projects (Murdoch and Slack 2002), the re-injection of drilling cuttings (Moschovidis et al. 2000), the heat production from geothermal reservoirs (Legarth et al. 2005) and more recently the CO_2 sequestration in deep geologic formations (Wawersik et al. 2001).

The hydraulic fracturing process involves the pumping of a viscous-fluid from a well into the rock formation under high enough fluid pressure to fracture the reservoir. In general, a fracture will re-orient itself in the complex stress field near the wellbore and will propagate further perpendicular to the minimum compressive stress. The pumping of fluid is maintained at

a rate high enough for the fluid pressure to overcome the minimum in-situ stress and hence to propagate the fracture. During the pumping process, proppant particles are gradually mixed with the fracturing fluid to ensure that the fracture will remain propped open when the pumping stops. A highly permeable channel will hence be formed for oil or gas to flow from the pay zone in the well (Economides and Nolte 2000).

Even in its most basic form, hydraulic fracturing is not a trivial process to model, as it involves the coupling of at least three physical processes: (i) the viscous flow of the fluid in the fracture (ii) the rock deformation of the surrounding medium induced by the fluid pressure on the fracture surfaces and (iii) the rock splitting and fracture propagation. Usually the solid deformation is modeled with the elasticity theory, which in analytic form can be represented by an integral equation that determines the non-local relationship between the fracture width and the fluid pressure. The fluid flow is modeled by lubrication theory, represented by a non-linear partial differential equation that relates the fluid flow velocity, the fracture width and the gradient of the pressure. The fracture propagation is assumed to take place when the stress intensity factor at the tip reaches a critical value equal with the rock fracture toughness which in many cases for rocks is assumed to be nearly zero.

In field operations, attention is focused on the prediction of the wellbore pressure which is normally measured during the treatment and is usually the only parameter available to evaluate and redesign the operation. Classical hydraulic fracturing simulators often underestimate the measured down-hole pressures. Research works involving surveying on net pressures (difference between the fracturing fluid pressure and the far-field confining stress) indicated that the net pressures encountered in the field are on average 50–70% higher than the predicted ones. These observations have triggered a series of dedicated studies which looked into the importance of the rock plastic deformation in hydraulic fracturing (Papanastasiou 1999a,b; Van Dam et al. 2002). All these studies had ignored the pressure diffusion and porous behavior of the rock deformation. Furthermore, although the cohesive model approach has been utilized by many authors in different disciplines, the physical interpretation of the process zone and its influence in hydraulic fracturing are still unexplored.

In examining the plentiful literature concerning fracture mechanics the cohesive zone modeling has attracted considerable attention, as it represents a powerful and efficient technique for computational fracture studies. The early conceptual works related to the cohesive zone model, were introduced by Barenblatt (1959, 1962) who proposed the cohesive zone model to investigate perfectly brittle materials. Dugdale (1960) adopted a fracture process zone to investigate ductile materials exhibiting small scale plasticity. Since then, a series of research work, to mention few (Hillerborg et al. 1976; Needleman 1987; Xu and Needleman 1994; Camacho and Ortiz 1996), have been oriented in the development of the cohesive zone concept in computational fracture mechanics. Xu and Needleman (1994) have presented a potential based cohesive zone model with cohesive elements that are inserted into a finite element mesh in advance and obeyed an exponential constitutive law in the normal direction. In this case, as the displacement-jump across the surface increases the traction increases to reach a maximum value and then it decays in a monotonic manner. Another modeling approach which has been proposed by Camacho and Ortiz (1996) was a stress based cohesive zone model where a new surface is adaptively created by duplicating nodes which were previously bonded. The work of Xu and Needleman (1994) has been widely used as it is easier to implement into a finite element analysis. Some limitations recognized in Xu and Needleman (1994) work, related to the imposed initial artificial compliance of the utilized cohesive zone law, were addressed by Geubelle and Baylor (1998) and Espinosa and Zavattieri (2003) who have adopted bilinear cohesive zone models by providing an adjustable initial slope in the cohesive law.

There are few studies utilizing the cohesive zone model in hydraulic fracturing. Some early studies in this area include the important work of Boone et al. (1986), Boone and Ingraffea (1990) in which they used the cohesive zone approach to model the fracture process in impermeable and permeable rocks. Other significant works include the use of the cohesive zone law to propagate fractures in order to investigate the inelastic behavior of rocks in hydraulic fracturing (Papanastasiou and Thiercelin 1993; Papanastasiou 1997, 1999a,b). Improving the research work in hydraulic fracturing, Schrefler et al. (2006) proposed a model, with a tip-velocity provided as part of the solution algorithm, and propagated successfully hydraulic fractures in an unknown path that may enucleate everywhere depending only on the stress and pressure fields.

In the present work, the fracture initiation and growth in porous media are analyzed with the cohesive zone approach as the fracture criterion (Barenblatt 1962; Hillerborg et al. 1976; Papanastasiou 1999a,b). Different types of models have been used for the mechanical behavior of the cohesive zone to account for rigid-softening to elastic-softening behavior of rocks. For all models the normal work of separation, which gives some indication of the implications of the cohesive surface characterization for fracture toughness in plane strain mode I fracture, is maintained the same. The resulting fracture shape with the cohesive zone, influence the pressure profile in the fracture and the stress distribution near the tip which in turn affects the overall characteristics (fracture length, width and propagation pressure) of a hydraulic fracture.

In this research work we investigated the influence of the constitutive cohesive zone characteristics on the size of process zone and consequently on the obtained results in hydraulic fracturing modelling. Furthermore, we demonstrate that the existence of the confining stresses influences further the size of the process zone. The resulting process zone is an important parameter that may explain partially the unexpected high fluid pressures observed in hydraulic fracturing field operations. This paper is organized in two parts as follows: In the first part, we describe the involved physical processes: the fluid flow, the rock deformation, the fracture propagation and the methodology that was adopted in the numerical model. In the second part, we present and critically evaluate the computational results and draw conclusions on the important parameters.

2 Methodology

The physical process of the fluid driven fracture involves the pumping of a viscous fluid that pressurizes the fracture surfaces which deform. Increasing the pressurization, critical loading conditions will be reached ahead of the tip splitting the rock and driving hydraulically the fracture. Thus, this process reveals that there is a strong coupling between the moving fluid, rock deformation and fracture propagation. Depending on the formation properties, in-situ stresses and pumping parameters, the fracture may propagate for more than hundred meters. In this study the fracture will propagate few meters, enough to extrapolate and reach correct conclusions for long-fractures. The propagation of a short fracture can also be used to interpret the results of the mini-frac calibration test that is carried out first in-situ for determining parameters such as the formation permeability and the closure stress that are further used for modelling the long hydraulic fractures.

In this section we describe the fully coupled numerical model for a fluid driven fracture in a porous rock that has been used to study the importance of the cohesive zone characteristics in hydraulic fracturing. The models were developed for plain strain geometry taking into consideration the symmetry conditions. This geometry is appropriate for modelling short fractures with fracture height relatively greater than the fracture length. Furthermore, this geometry is also appropriate for examining tip effects since the deformation of any arbitrary fracture shape is approximately planar near the tip. The fracture propagates perpendicular to the minimum in situ stress and remains planar. This predefined path for the propagation is also convenient with the cohesive zone numerical approach (Papanastasiou 1999a,b).

2.1 Fluid-flow

The fluids that are used in hydraulic fracturing are normally power-law with shear-thinning behavior which means that the viscosity decreases with increasing shear rate. In order to avoid this complex fluid behavior, a simple appropriate model for fluid flow in a fracture is embodied in lubrication theory. It assumes laminar flow (uniformly viscous Newtonian), the fluid is incompressible and it accounts for the time dependent rate of crack opening. The continuity equation which imposes the conservation of mass in one dimensional flow is (Boone and Ingraffea 1990)

$$\frac{\mathrm{d}q}{\mathrm{d}x} - \frac{\mathrm{d}w}{\mathrm{d}t} + q_l = 0 \tag{1}$$

where q is the local flow rate along the fracture in direction x, q_l is the local fluid loss in rock formation and w is the crack opening. Equation (1), which accounts for the fluid leak-off from the fracture surface into the rock formation, can be used to determine the local flow rate q.

The second equation is derived from the conservation of momentum balance. For a flow between parallel plates the lubrication equation, which relates the pressure gradient to the fracture width for a Newtonian

fluid of viscosity μ, yields (Boone and Ingraffea 1990)

$$q = uw = -\frac{w^3}{12\mu}\frac{\mathrm{d}p}{\mathrm{d}x} \tag{2}$$

where p denotes the fluid pressure and u the average velocity of the fluid over a cross-section of the fracture. Equation (2) determines the pressure profile along the fracture from the local width and local flow rate. According to Eq. (2), the pressure gradient and hence the solution, is very sensitive to fracture width. Therefore, the largest part of the pressure drop takes place within a small area near the tip where the width decreases significantly before it vanishes at the tip.

2.2 Rock deformation

The basic theory of poroelasticity in which the resulting fully coupled linear quasi-static field equations were derived, was initially introduced by the pioneering work of Biot (1941). Since then, many researchers have contributed to its further development. The theory is commonly applied to soil mechanics problems especially for consolidation problems. The Biot poroelastic theory was reformulated in a more physically relevant manner to account for poroelastic effects by Rice and Cleary (1976). For the definition of a poroelastic system, five material constants are required. These material constants include the drained shear modulus G, the drained Poisson ratio ν, the undrained Poisson ratio ν_u, the Skempton's pore pressure coefficient B and the intrinsic permeability κ (Darcies). Rice and Cleary (1976) have successfully linked these constants to micromechanical parameters that can be easily obtained for any soil or rock type material. These micromechanical parameters are the porosity n, the fluid bulk modulus K_f, the solid grain bulk modulus K_s, the porous bulk modulus for the solid skeleton K, the Poisson ratio ν and the permeability k.

The total stresses σ_{ij} are related to the effective stresses σ'_{ij} through

$$\sigma_{ij} = \sigma'_{ij} - ap \tag{3}$$

The effective stresses govern the deformation and failure of the rock. The poroelastic constant a, is independent of the fluid properties and it is defined as

$$\alpha = \frac{3(\nu_u - \nu)}{B(1-2\nu)(1+\nu_u)} = 1 - \frac{K}{K_s} \tag{4}$$

As it is mentioned before, this theory is commonly applied in soils. An important distinction when applying this formulation to rock is to consider the compressibility of the constitutive materials. For Soils B and α are equal to unity but in rocks are significantly less than one.

The problem is stated here using the effective stress principle for porous media and the solution is limited to a 2-D context. The theory of poroelasticity can be approximated numerically using the finite element method and a standard Galerkin formulation as described in Zienkiewicz (1984) and Lewis and Schrefler (2000). The finite element equations in matrix notation are as following (Boone and Ingraffea 1990)

$$[K]\{u\} + [L]\{p\} = \{F\} \quad \text{(Stiffness equation)} \tag{5}$$

$$[S]\{\dot{p}\} + [L]^T\{\dot{u}\} + [H]\{p\} = \{q\} \quad \text{(Flow equation)} \tag{6}$$

where u are the nodal displacements, p are the nodal pressures, F are the nodal forces, q are the nodal flows, $[K]$ is the stiffness matrix, $[L]$ is the coupling matrix, $[H]$ is the flow matrix and $[S]$ is the compressibility matrix. In a descritized form the unknown field parameters u and p are substituted by the nodal values and the interpolation functions which enter in the calculation of the matrices as

$$p = N^p\{p\}, \quad u = N^u\{u\}, \quad \varepsilon = B\{u\} \tag{7}$$

where N^p and N^u are the nodal shape functions for pressure and displacements, respectively. B is the matrix for the strain ε that contains the derivatives of the displacement interpolation functions. The definitions of matrices in the system of Eqs. (5), (6) in a 2-D formulation are given by the following expressions

$$\begin{aligned}
[K] &= \int_\Omega B^T D B \mathrm{d}\Omega, \quad [L] = a\int_\Omega N^u \begin{Bmatrix} d/\mathrm{d}x \\ d/\mathrm{d}y \end{Bmatrix} N^p \mathrm{d}\Omega \\
[S] &= \int_\Omega (N^p)^T \frac{1}{Q} N^p \mathrm{d}\Omega, \\
[H] &= \kappa \int_\Omega N^u \begin{Bmatrix} d/\mathrm{d}x \\ d/\mathrm{d}y \end{Bmatrix} N^p \Bigg]^{\mathrm{T}} \begin{pmatrix} d/\mathrm{d}x \\ d/\mathrm{d}y \end{pmatrix} N^p \mathrm{d}\Omega
\end{aligned} \tag{8}$$

where D is the drained material elasticity matrix. The quantity $1/Q$ takes the following forms

$$\begin{aligned}
\tfrac{1}{Q} &= \left(\frac{\phi}{K_f} + \frac{1-\phi}{K_s} - \frac{1-a}{K_s}\right), \\
\tfrac{1}{Q} &= \frac{\alpha(1-\alpha B)}{BK}, \\
\tfrac{1}{Q} &= \frac{9(\nu_u - \nu)(1-2\nu_u)}{2GB^2\kappa(1-2\nu)(1+\nu_u)^2}
\end{aligned} \tag{9}$$

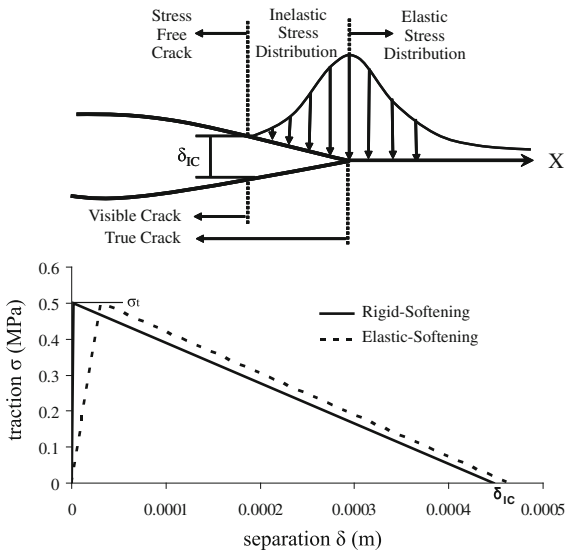

Fig. 1 Representation of the fracture process and the constitutive cohesive zone law

2.3 Fracture propagation

There is number of fracture propagation criteria provided by the theory of fracture mechanics. The criterion for fracture propagation is usually given either by conventional energy approach which states that a fracture propagates when the energy release rate reaches a critical value related to fracture toughness or by the stress intensity approach which states that a fracture propagates when the stress intensity factor at the tip exceeds the rock toughness. The energy release rate and stress intensity approaches are essentially equivalent and uniquely related for linear elastic materials. The most robust criterion for non-linear mechanics is described by the cohesive zone constitutive model. The cohesive zone model approach should be clearly contrasted with the conventional fracture mechanics based infinitely sharp fracture models; as such fracture models have led to a physically meaningless singular stress field near the fracture tip. The cohesive zone is a region ahead of the crack tip that is characterized by micro-cracking along the crack path. The main fracture is formed by inter connection of these micro cracks. The cohesive zone model implies that normal stress continues to be transferred across a discontinuity which may or may not be visible as shown in Fig. 1. This stress is determined from the softening stress-strain relation that various rocks exhibit in calibrations tests. This transferred normal stress is a function of the separation and falls to zero at a critical opening and then the fracture propagates. The evolution of the crack is governed by energy balance between the work of the external loads and the sum of the bulk energy of the uncracked part and the energy dissipated in the fracture process. The main mathematical difficulty is given by the fact that the fracture energy depends on the opening of the distributed micro-cracks. To simplify the mathematical difficulties, it is assumed that the cohesive zone localizes, due to its softening behavior, into a narrow band ahead of the visible crack.

The constitutive behavior of the cohesive zone is defined by the traction-separation relation derived from laboratory tests. The traction-separation constitutive relation for the surface is such that with increasing separation, the traction across this cohesive surface reaches a peak value and then decreases and eventually vanishes, permitting for a complete separation. Simple cohesive zone models can be described by two independent parameters which are usually, for mode-I plane strain, the normal work of separation or the fracture energy G_{IC} and either the tensile strength σ_t or the complete separation length δ_{IC}. An additional parameter in these models is the slope of the initial loading which may define a range from rigid-softening to elastic-softening response under tensile stress-state.

In order to investigate the main characteristics of this curve we carried out computations for different initial slopes to simulate a rigid-softening to elastic softening behavior. The transition from the elastic softening to the rigid-softening was carried out by increasing the initial slope of the constitutive cohesive law by five times in each model. The case of the most rigid behavior corresponds to twenty times the stiffness of the most elastic case. In all cases the area under the curve which is related to the work of separation is maintained the same (Fig. 1b).

The area under the traction-separation curve equals with fracture energy G_{IC} which is the work needed to create a unit area of fully developed crack. For elastic solids this energy is related to the rock fracture toughness K_{IC} through (Rice 1968; Kanninen and Popelar 1985)

$$K_{\mathrm{IC}}^2 = \frac{G_{\mathrm{IC}} E}{1-\nu^2} \tag{10}$$

where E is the young modulus and ν is the Poisson ratio. The rock fracture toughness can be calculated from laboratory tests. For the case of the rigid-softening

behavior the traction-separation relation is uniquely determined by

$$\sigma = \sigma_t(1 - \delta/\delta_{\mathrm{IC}}) \tag{11}$$

where σ_t is the uniaxial tensile strength of the rock and δ_{IC} is the critical opening displacement at which σ falls to zero. The value of δ_{IC} is given by (Kanninen and Popelar 1985)

$$\delta_{\mathrm{IC}} = \frac{2K_{\mathrm{IC}}^2(1-\nu^2)}{E\sigma_t} \tag{12}$$

For the case of the elastic loading the cohesive constitutive relations were augmented and modified to take into account the initial part of the curve as follows

$$\sigma = \sigma_t\left(\frac{\delta}{\delta_{\mathrm{el}}}\right) \tag{13}$$

with the limit of elastic deformation is given by

$$\delta_{\mathrm{el}} = \frac{\sigma_t}{k_n} \tag{14}$$

where k_n is the stiffness of the traction-separation relation in the loading regime with units of [MPa/m]. In the post-peak softening regime the cohesive constitutive relation is given by

$$\sigma = \sigma_t\left[1 - \frac{(\delta - \delta_{\mathrm{el}})}{(\delta_{\mathrm{IC}} - \delta_{\mathrm{el}})}\right] \tag{15}$$

To further investigate the influence of the cohesive zone law in hydraulic fracturing, we have also studied different forms of softening behavior. For this purpose we have utilized an exponential softening that is described by:

$$D^{\mathrm{Exponential}} = \left\{\frac{1 - e^{-\alpha\left(\frac{\delta-\delta_{\mathrm{IC}}}{\delta_{\mathrm{IC}}-\delta_{\max}}\right)}}{1 - e^{-\alpha}}\right\} \tag{16}$$

The above parameter is controlled by the exponential coefficient α. We have conducted a parametric study for this variable with values of $\alpha = 1, 2, 3, 4$. The value of the exponent α gives a measure of the curvature of the softening equation that enters in the traction-separation equation to yield

$$\sigma = \left(1 - D^{\mathrm{Exponential}}\right)\sigma_t \tag{17}$$

The critical value of the crack opening displacement is uniquely determined from Eq. (17). The graphical representation of the new constitutive behavior for different exponent values and the case of linear elastic-softening, for comparison, are shown in Fig. 2. The loading part of the cohesive constitutive law was kept the same ($k_n = 1$) and the softening part was parametrically investigated as it will be described in Sect. 4.

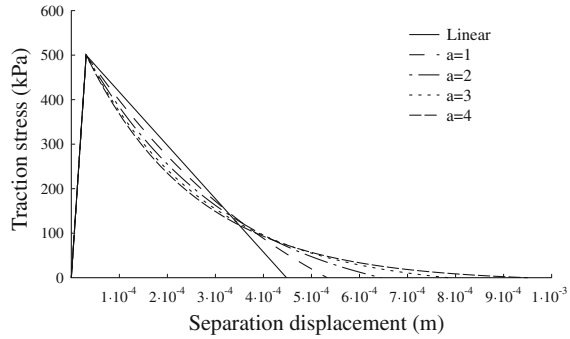

Fig. 2 Exponential constitutive laws for softening

3 Numerical implementation

The governing equations were discretized in space with the finite element method and in time with the finite difference method. Linear interpolations were used for the approximation of both displacement and the pore pressure degrees of freedom. The sharp changes that are expected in the geometry of the propagating tip, is dealt with placing a sufficient fine mesh around the predefined fracture path so as to ensure numerical accuracy. No special re-meshing scheme was used as the mesh was defined to be sufficiently fine along the fracture.

The calculations were carried out in Abaqus using 4-node plain strain isoparametric elements to model the domain and 6-node cohesive elements to model the fluid flow in the fracture and the fracturing process (Abaqus 2006). The cohesive elements were enhanced with two additional nodes for the modeling of the fluid flow. The cohesive zone approach cancels the stress singularity when the separation at the tail of the cohesive zone law reaches a critical value at which the cohesive traction vanishes. Furthermore, this cancels the coupled fluid pressure singularity that is encountered in the analytic framework of the fluid driven problem. Sinclair (1996) showed that the cohesive traction-separation laws cancel the opening singularity produced by loading remotely from the fracture with the closing singularity produced by cohesive stresses on the fracture flanks near the fracture tip. The descritized domain area was considered to be a 30 m × 30 m and the predefined path of the fracture was defined to be 11 m along which the cohesive elements were laid to save computational time. The geometry and the resulting discretization are shown in Fig. 3.

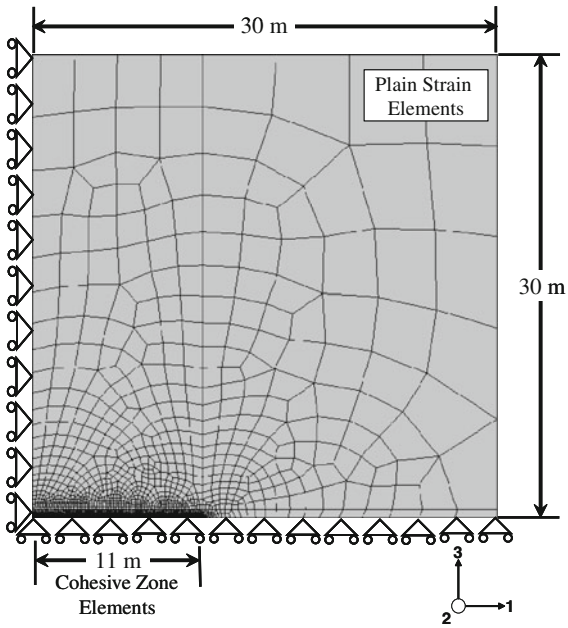

Fig. 3 Geometry, boundary conditions and discretized domain

Table 1 Input parameters for the computational examples

Variable	Value
Rock properties	
Young modulus, E (MPa)	16200
Poisson ratio, ν	0.3
Pumping parameters	
Viscosity, μ (kPa s)	0.0001
Injection rate, q (m^3/s m)	5.00E-06
Domain permeability, k (m/s)	5.88E-10
In situ stress field (effective)	
Maximum, σ_1 (MPa)	14
Intermediate, σ_2 (MPa)	9
Minimum, σ_3 (MPa)	3.7
Initial conditions	
Void ratio, e	0.333
Pore pressure, (MPa)	1.85
Initial gap, (perforation)- (m)	0.1

The wellbore location is at the left-lower corner and the fracture is assumed to grow in both directions along the axis-1. For a long fracture the size of the wellbore is negligible and is usually ignored in the modeling. This remark, along with the condition that the wellbore is cased, cemented and fully bonded with the rock formation, justifies the use of symmetry conditions within a reasonable accuracy (Fig. 3). The in-situ stresses were inserted as initial stresses and by applying the equilibrium load at the far right and top edges. At the top edge a value of $\sigma_3 = 3.7$ MPa was applied parallel to axis-3 as the minimum in situ stress or closure stress perpendicular to the fracture surfaces. The fracture will propagate along the axis-1 which is parallel to the maximum in situ stress $\sigma_1 = 14$ MPa. An initial condition is also required for defining an initial fracture length for the flow. This length was considered 0.1 m, approximately equals with the perforation length from where the fractures initiate. The in-situ stresses and the initial conditions are applied in the first step to achieve system equilibrium before the propagation starts.

4 Analysis and results

In this section we present results of the analysis to demonstrate the importance of the cohesive zone in modeling hydraulic fracturing in both elastic and porous elastic solids. The parameters upon which the numerical computations were based are given in Table 1. These parameters include the rock properties, the pumping parameters, the in-situ stress field and the initial conditions. The only extra parameter that is needed to consider poroelastic deformation and propagation of the poroelastic fracture is the pore pressure of the domain requiring an extra degree of freedom at the nodes of the plain strain elements. For comparison of the results, the total stress field was applied in the poroelastic analysis whereas for the non-porous models the corresponding effective stress field was applied.

In order to investigate the main characteristics of the cohesive zone law, we conducted parametric analyses for its constitutive behavior to simulate the changes from rigid-softening to elastic-softening behavior. The constitutive response of the rigid-softening corresponds to a strong rock formation whereas the elastic-softening corresponds to a soft rock formation. For simplicity we have named these four cases as $k_n = 1$, 5, 10, 20 to correspond the times that the slope of the loading branch has been multiplied to meet the constitutive behavior that we have mentioned. The shape of the constitutive law is shown in Fig. 1b where for clarity reasons only the investigated two extreme cases were plotted. The case of k_n ($\times 1$) corresponds to

Table 2 Cohesive zone properties

Uniaxial tensile strength, σ_t (MPa)	0.5
Loading stiffness k_n (MPa/m)	16,200/81,000/ 162,000/324,000
Fracture energy, G_{IC} (kPa m)	0.224
Permeability of cohesive zone, q_b (m/s)	0/5.879E-10

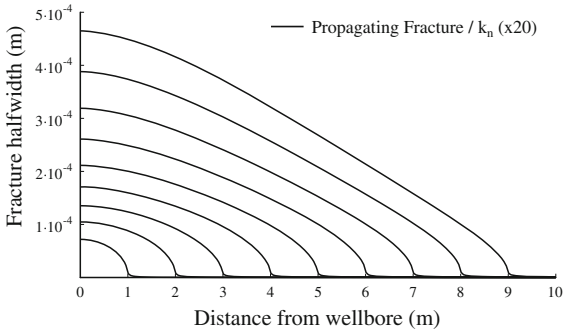

Fig. 4 Fracture profiles of a propagating fracture

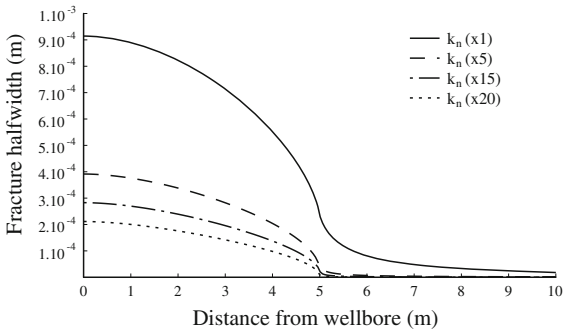

Fig. 5 Fracture apertures for different values of the loading slope of the constitutive cohesive law

elastic-softening behavior and the k_n ($\times 20$) to rigid-softening. The properties of the cohesive zone are summarized in Table 2. These properties include the uniaxial tensile strength, the fracture energy which is the area under the traction-separation curve calculated to meet an equivalent fracture toughness of 2 MPa $m^{1/2}$, the permeability of the elements and the parametrically investigated loading slope of the first branch of the cohesive constitutive law.

All the results presented next correspond to fractures at the state of propagation. The fractures were propagated from an initial length of 0.1 m to reach 9 m long. For example, Fig. 4 shows the profile of a propagating fracture at different lengths every 1 m interval.

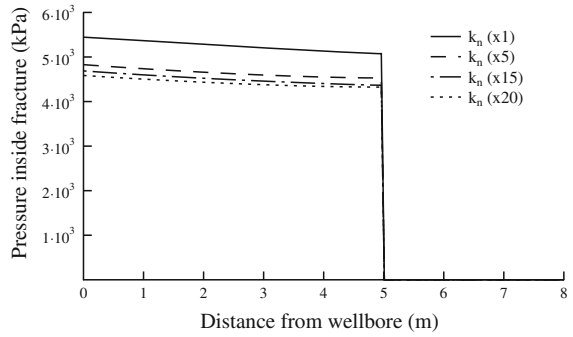

Fig. 6 Fluid-pressures in the fractures for different values of the loading slope of the constitutive cohesive law

Figure 5 shows the obtained half-width of a fracture in an elastic solid for cases of different loading slope of the cohesive constitutive relation after the fracture reached a length of 5 m. The calculated width of the propagating elastic-softening, which corresponds to k_n ($\times 1$), is much larger than the calculated width of the rigid-softening which corresponds to k_n ($\times 20$). The cusping of the fracture profiles is larger for the case of elastic-softening indicating a ductile behavior.

The results of the rigid-softening are similar to a brittle behavior or to a pure elastic fracture without a process zone. The differences in the results are the outcome of the cohesive zone models which were incorporated as the fracture propagation criterion.

Figure 6 shows the corresponding pressure profile in the fractures when the visual tip reached a distance of 5 m. The fluid front position is found to be at the point where the fluid pressure changes sign or falls to zero. It was assumed in these computations that the formation domain and the process zone are impermeable and the pressure drop takes place mainly at the visual tip for these specific parameters.

Figure 7 shows the net-pressure (pressure in the fracture—remote confining stress) during fracture propagation. Higher pressure is needed to propagate the fracture with elastic-softening cohesive behavior. The pressure drop is more pronounced in the case of the elastic-softening behavior compared to the pressure drop in the case of the rigid-softening behavior. However, as Fig. 7 suggests, for very long fractures is expected that the net-pressure for all cases will tend to zero as the length of the process zone diminishes compared to the fracture length.

Figure 8 shows the distribution of the cohesive stress (stress transferred normal to the propagation direction)

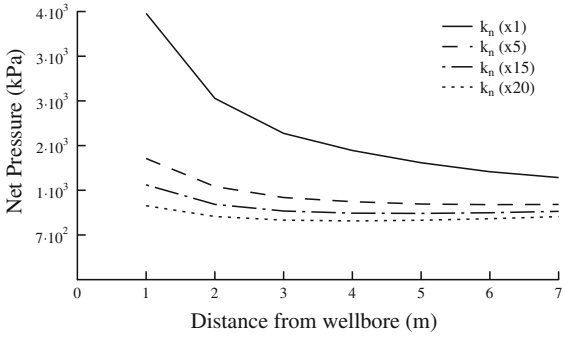

Fig. 7 Net-pressures vs fracture length for different values of the loading slope of the constitutive cohesive law

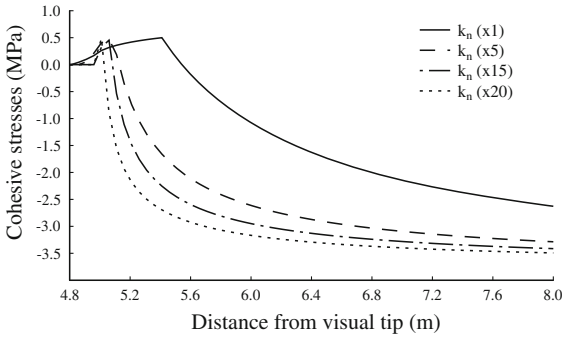

Fig. 8 Distribution of cohesive stress (normal to propagation direction) in front of the fracture for different values of the loading slope of the cohesive law

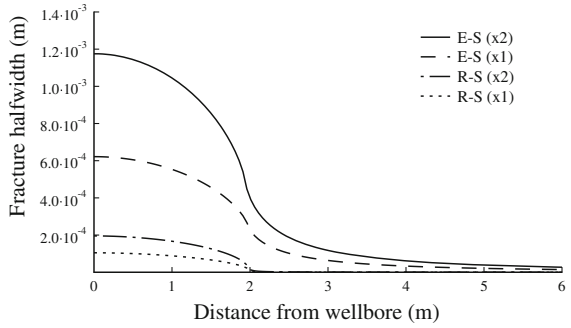

Fig. 9 Influence of the in-situ stress field on the fracture apertures for elastic-softening (*E-S*) and rigid-softening (*R-S*) cohesive laws. The cases marked with X2 correspond to a double value of the confining stresses

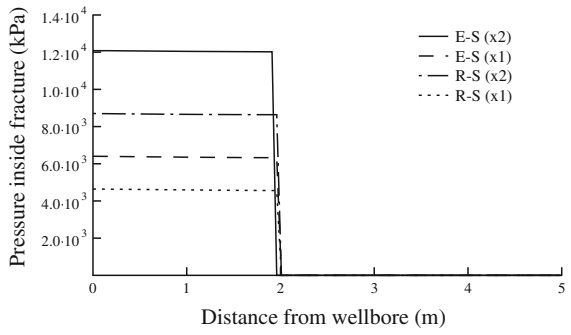

Fig. 10 Influence of the in-situ stress field on the pressure distributions for elastic-softening (*E-S*) and rigid-softening (*R-S*) cohesive laws

in front of the fractures for the different values of the loading slope of the constitutive cohesive model. The results reveal that the tensile stress is contained in a small region near the tip with its maximum value equal to the assumed tensile strength of the rock. During the fracturing process there is a relief of the compressive stresses ahead of the fracture tip followed by a complete separation when the crack-opening reaches the critical value defined in the propagation criterion. The elastic-softening model generates much longer process zone compared to the rigid-softening model. The short process zone generated by the rigid-softening model suggests that its results can be compared for validation with the results of an elastic fracture loaded with a uniform internal pressure. It seems that the loading slope of the constitutive cohesive model influences to a large extent the size of the generated process zone in hydraulic fracturing and as a result wider fractures are generated and higher pressures are needed for propagating an elastic-softening cohesive fracture.

Furthermore, we investigated the role of the confining stresses in hydraulic fracturing. It was suggested that the existence of the confining stresses in field conditions may increase the resistance of rock to fracturing leading to an apparent increase of the fracture toughness. We repeated the calculations of the two extreme cases, for rigid-softening and elastic-softening for a stress field where the confining stresses were doubled. Figure 9 shows that the fracture width profiles were almost doubled when the confining stresses were doubled for both rigid-softening and elastic-softening models. Figure 10 shows the corresponding pressure profiles in the fractures for the two cohesive material models and for the different confining stresses. These results are better compared in Fig. 11 where the net-pressures are plotted. Apparently in a field with high confining stresses, higher net-pressure is needed for creating a hydraulic fracture and a wider fracture is created.

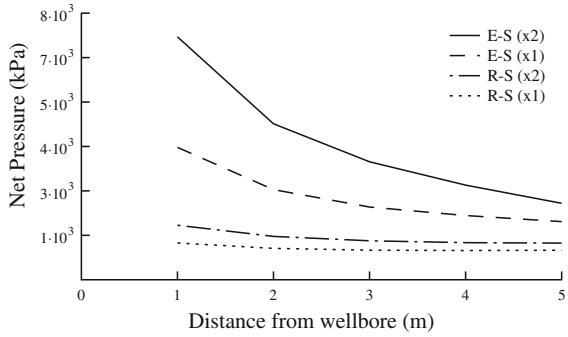

Fig. 11 Influence of the in-situ stress field on the elastic net pressures for elastic-softening (*E-S*) and rigid-softening (*R-S*) cohesive laws

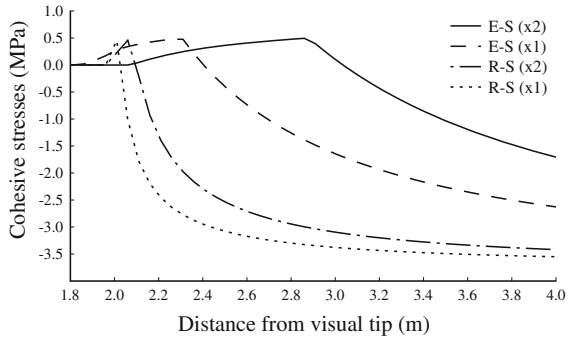

Fig. 12 Influence of the in-situ confining stresses on the cohesive stresses in front of the fractures for elastic-softening (*E-S*) and rigid-softening (*R-S*) cohesive laws

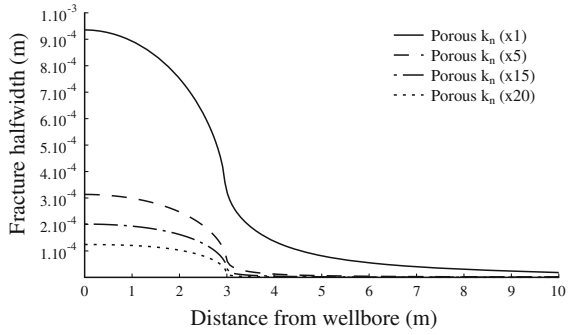

Fig. 13 Aperture of porous-elastic fractures for different values of the loading slope of the cohesive laws

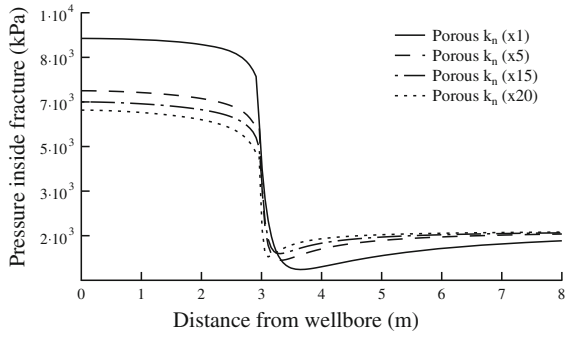

Fig. 14 Pressure profile in the porous-elastic fractures for different loading slope of the cohesive law

We emphasize again that the differences in the results of Figs. 9, 10, 11 are due to the longer process zone which is created under higher confining stresses as clearly shown in Fig. 12. However, the difference in the results is expected to diminish with increasing fracture length but there are many applications where short hydraulic fractures are created in weak rock formations.

Computations were also carried out for hydraulic fracturing in a porous material taking into account the fluid diffusion in the surrounding formation. The results were compared with the results from the non-porous material where fluid diffusion and leak-off in the formation were ignored. The objective of these calculations was to investigate further how the results of the cohesive model will be affected by the existence and the changes of the pore pressure in the formation. Figure 13 shows the half-width of a propagating fracture in the poroelastic solids for the cases of different loading slope of the cohesive constitutive law after the fracture reached a length of 3 m. Comparing the results of Fig. 5 for the non-porous fracture, with the results of Fig. 13 for the porous fracture it is evident that the porous fracture profiles are wider especially for the case of the elastic-softening cohesive model whereas for the case of the rigid-softening behavior the difference is negligible. The porous fractures reached about the same width at a shorter length (3 m) compared to a longer length (5 m) for the non-porous fractures.

Figure 14 shows the pressure profile in the fracture and process zone during propagation when the visual tip reached a distance of 3 m. The fluid-pressure drops abruptly near the visual tip. The pressure ahead of the fracture tip decreases to values below the initial formation pressure and far away from the tips tends asymptotically to its initial undisturbed value (1.85 MPa).

Figure 15 shows the net-pressure (pressure in the fracture—remote confining stress) during fracture propagation as a function of the fracture length for the porous models. In comparison with Fig. 7, the required net-pressure that is needed for propagating the

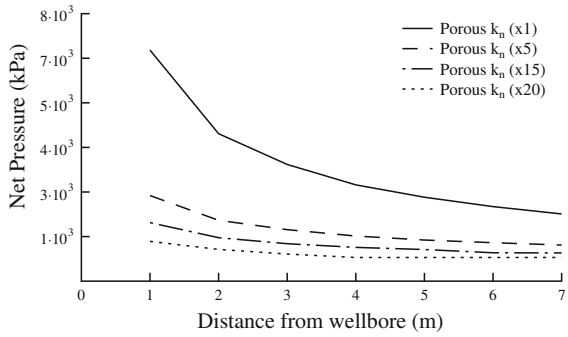

Fig. 15 Net-pressures for porous-elastic fractures for different loading slope of the cohesive law

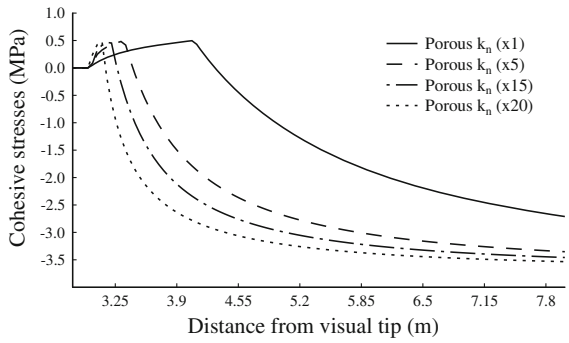

Fig. 16 Distribution of stress normal to the propagation direction for porous models

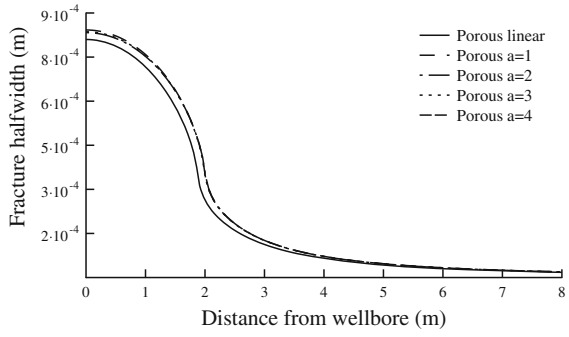

Fig. 17 Width-profiles for porous elastic fractures with different form of exponential softening

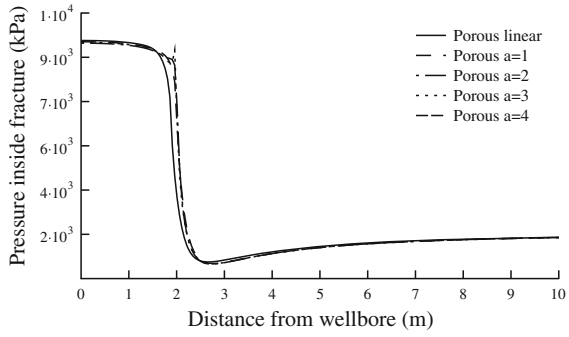

Fig. 18 Pressure distributions in the porous-elastic fractures for different form of exponential softening

porous fracture is higher than the net-pressure required for propagating the non-porous fracture, especially for short propagations.

In order to estimate the size of the cohesive zone in the porous models we plotted in Fig. 16 the profile of the stress normal to the propagation direction ahead of the fracture tip. It is observed again that the process zone size is much larger in the case of the elastic-softening behavior, especially in the case of the porous model, suggesting that the pore-pressure in the formation has a strong interaction with the stress concentration near the fracture tip. It is noted that although a linear softening behavior in the cohesive model was implemented, the calculated stress profiles from the resulting separations are sufficient non-linear. This outlines the adequacy of simple softening relations in capturing the non-linear stress distribution ahead of the crack tip.

In the next computations we investigated the influence of the exponential softening form described by Eqs. (16), (17) and depicted in Fig. 2 on the required propagation pressures and fracture dimensions of the created fractures. Figure 17 shows the half-width of a propagating fracture in poroelastic solids for cases of different exponential softening. It is clear that the exact form of the exponential softening does not influence to a great degree the fracture profiles as well the pressure profile in the fracture (Fig. 18).

Figure 19 shows the distribution of the cohesive stress (stress transferred normal to the propagation direction) in front of the fractures for the different values of the exponential softening in the constitutive cohesive model. The results reveal that the form of the exponential softening changes slightly the stress profile in the process zone but the size of the process zone remains nearly unaffected.

5 Conclusions

We studied the influence of the cohesive zone characteristics on the modeling of hydraulic fracturing technique. The objective was to explain, at least partially, the elevated pressures that are needed to propagate the fractures in the field and they are not correctly predicted by the conventional models. In order to keep the

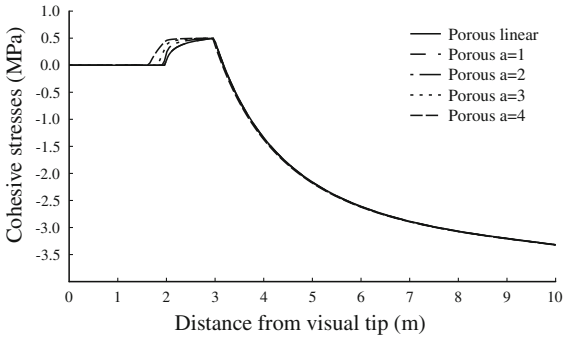

Fig. 19 Distribution of stress normal to the propagation direction for porous models and different form of exponential softening

model parameters to a minimum, rigid-softening and elastic-softening cohesive relations were considered to represent the splitting process of the rock near the fracture tip. A set of fully coupled models for the fluid-flow in the fracture, the rock deformation and the fracturing process were implemented and solved numerically with the finite element code Abaqus.

From the analysis conducted, we found that for propagating a fracture with an elastic-softening cohesive model higher pressure is needed and the created fracture is wider compared to the case of a rigid-softening cohesive model. These results are due to the larger process zone obtained with the elastic-softening model. Furthermore, we showed that the exact form of the softening branch of the cohesive model has no significant influence on the obtained results. We found that the existence of the confining stresses increases the size of the process zone and results in wider fractures and higher propagation pressures. The changes in the pore pressure during fracturing, increase further the size of the process zone which in turn increase the propagation pressures and the dimensions of the created fractures.

Acknowledgements The authors would like to acknowledge the Cyprus Research Promotion Foundation for funding this research through the program ENIΣX/0505/31.

References

Abaqus (2006) Version 6.6 Manuals

Adachi J, Siebrits E, Peirce A, Desroches J (2007) Computer simulation of hydraulic fractures. Int J Rock Mech Min Sci 44:739–757

Adachi J, Detournay E (2008) Plain strain propagation of a hydraulic fracture in permeable rock. Eng Frac Mech 75:4666–4694

Barenblatt GI (1959) The formation of equilibrium cracks during brittle fracture: general ideas and hypothesis, axially symmetric cracks. Appl Math Mech (PMM) 23:622–636

Barenblatt GI (1962) The mathematical theory of equilibrium cracks in brittle fracture. Adv Appl Mech 7:55–129

Biot MA (1941) General theory of three dimensional consolidation. J Appl Phys 12:155–164

Boone TJ, Wawrzynek PA, Ingraffea AR (1986) Simulation of fracture process in rock with application to hydrofracturing. Int J Rock Mech Min Sci Geomech Abstr 23:255–265

Boone JT, Ingraffea AR (1990) A numerical procedure for simulation of hydraulically driven fracture propagation in poroelastic media. Int J Numer Anal Methods Geomech 14:27–47

Camacho GT, Ortiz M (1996) Computational modeling of impact damage in brittle materials. Int J Solils Struct 33:2899–2938

Dugdale DS (1960) Yielding of steel sheets containing slits. J Mech Phys Solids 8:100–104

Economides M, Nolte K (2000) Reservoir stimulation. Wiley, Chichester

Espinosa HD, Zavattieri PD (2003) A grain level model for the study of failure initiation and evolution in polycrystalline brittle materials. Part I: theory and numerical implementation. Mech Mater 35:333–364

Geubelle PH, Baylor JS (1998) Impact induced delamination of composites: 2D simulation. Compos Part B 29:589–602

Hillerborg A, Modeer M, Petersson PE (1976) Analysis of crack formation and crack growth in concrete by means of fracture mechanics and finite elements. Cem Concr Res 6:773–782

Jeffrey RG, Settari A, Mills KW, Zhang X, Detournay E (2001) Hydraulic fracturing to induce caving: fracture model development and comparison to field data. In: Elsworth D, Tinucci JP, Heasley KA (eds.) Rock mechanics in the national interest-proceedings of the 38th US rock mechanics symposium, Lisse Balkema 1:251–259

Kanninen MF, Popelar CH (1985) Advanced fracture mechanics. Oxford University Press, NY

Legarth B, Huenges E, Zimmermann G (2005) Hydraulic fracturing in sedimentary geothermal reservoir: results and implications. Int J Rock Mech Min Sci 42:1028–1041

Lewis RW, Schreffler BA (2000) The finite element method in the static and dynamic deformation and consolidation of porous media. Wiley, London

Moschovidis Z et al. (2000) The Mounds drill-cuttings injection experiment: final results and conclusions. In: Proceedings of the IADC/SPE drilling conference. Richardson: Society of Petroleum Engineers; [SPE 59115]

Murdoch LC, Slack WW (2002) Forms of hydraulic fractures in shallow fine grained formations. J Geotech Geoenviron 128:479–487

Needleman A (1987) A continuum model for void nucleation by inclusion debonding. ASME J Appl Mech 54:525–531

Papanastasiou P, Thiercelin M (1993) Influence of inelastic rock behavior in hydraulic fracturing. Int J Rock Mech Min Sci Geomech Abstr 30:1241–1247

Papanastasiou P (1997) The influence of plasticity in hydraulic fracturing. Int J Fract 84:61–79

Papanastasiou P (1999a) An efficient algorithm for propagating fluid driven fractures. Comput Mech 24:258–267

Papanastasiou P (1999b) The effective fracture toughness approach in hydraulic fracturing. Int J Fract 96:127–147

Rice JR (1968) A path independent integral and the approximate analysis of strain concentration by notches and cracks. J Appl Mech 57:379–386

Rice JR, Cleary MP (1976) Some basic stress diffusion solutions for fluid-saturated elastic porous media with compressible constituents. Rev Geophys Space Phys 14:227–241

Schrefler BA, Secchi S, Simoni L (2006) On adaptive refinement techniques in multi-field problems including cohesive fracture. Comput Methods Appl Mech Eng 195:444–461

Sinclair GB (1996) On the influence of cohesive stress-separation laws on elastic stress singularities. J Elast 44:203–221

Spence DA, Turcotte DL (1985) Magma-driven propagation crack. J Geophys Res 90:575–580

Van Dam DB, Papanastasiou P, De Pater CJ (2002) Impact of rock plasticity on hydraulic fracture propagation and closure. J Prod Facil (SPE 78812) 17(3):149–159

Wawersik WR, Rudnicki JW, Dove P, Harris J, Logan JM, Pyrak-Nolte L, Orr Jr FM, Ortoleva PJ, Richter F, Warpinski NR, Wilson JL, Wong TF (2001) Terrestrial sequestration of CO_2: an assessment of research needs. Adv Geophys 43: 97–177

Xu X-P, Needleman A (1994) Numerical simulations of fast crack growth in brittle solids. J Mech Phys Solids 42(9):1397–1434

Zienkiewicz OC (1984) Coupled problems and their numerical solution. In: Lewis RW, Bettess P, Hinton E (eds) Numerical methods in coupled systems. Wiley, London